Engineering a Camelid Antibody Fragment That Binds to the Active Site of Human Lysozyme and Inhibits Its Conversion into Amyloid Fibrils†

Pak-Ho Chan,‡ Els Pardon,§,|| Linda Menzer,‡,⊥ Erwin De Genst,‡,§ Janet R. Kumita,‡ John Christodoulou,‡ Dirk Saerens,||,# Alain Brans,⊥ Fabrice Bouillenne,⊥ David B. Archer,+ Carol V. Robinson,‡ Serge Muyldermans,||,# André Matagne,⊥ Christina Redfield,○ Lode Wyns,§,|| Christopher M. Dobson,*,‡ and Mireille Dumoulin*,‡,⊥

Department of Chemistry, University of Cambridge, Lensfield Road, Cambridge CB2 1EW, U.K., Laboratorium voor Ultrastructuur, Vrije Universiteit Brussel, Pleinlaan 2, 1050 Brussels, Belgium, Department of Molecular and Cellular Interactions, VIB, Vrije Universiteit Brussel, Pleinlaan 2, 1050 Brussels, Belgium, Laboratoire d'Enzymologie, Centre d'Ingénierie des Protéines, Institut de Chimie B6, Université de Liège, B-4000 Liège (Sart Tilman), Belgium, Laboratorium voor Cellulaire en Moleculaire Immunologie, Vrije Universiteit Brussel, Pleinlaan 2, 1050 Brussels, Belgium, School of Biology, University of Nottingham, University Park, Nottingham NG7 2RD, U.K., and Department of Biochemistry, University of Oxford, South Parks Road, Oxford OX1 3QU, U.K.

Received April 3, 2008; Revised Manuscript Received July 14, 2008

ABSTRACT: A single-domain fragment, cAb-HuL22, of a camelid heavy-chain antibody specific for the active site of human lysozyme has been generated, and its effects on the properties of the I56T and D67H amyloidogenic variants of human lysozyme, which are associated with a form of systemic amyloidosis, have been investigated by a wide range of biophysical techniques. Pulse-labeling hydrogen−deuterium exchange experiments monitored by mass spectrometry reveal that binding of the antibody fragment strongly inhibits the locally cooperative unfolding of the I56T and D67H variants and restores their global cooperativity to that characteristic of the wild-type protein. The antibody fragment was, however, not stable enough under the conditions used to explore its ability to perturb the aggregation behavior of the lysozyme amyloidogenic variants. We therefore engineered a more stable version of cAb-HuL22 by adding a disulfide bridge between the two β-sheets in the hydrophobic core of the protein. The binding of this engineered antibody fragment to the amyloidogenic variants of lysozyme inhibited their aggregation into fibrils. These findings support the premise that the reduction in global cooperativity caused by the pathogenic mutations in the lysozyme gene is the determining feature underlying their amyloidogenicity. These observations indicate further that molecular targeting of enzyme active sites, and of protein binding sites in general, is an effective strategy for inhibiting or preventing the aberrant self-assembly process that is often a consequence of protein mutation and the origin of pathogenicity. Moreover, this work further demonstrates the unique properties of camelid single-domain antibody fragments as structural probes for studying the mechanism of aggregation and as potential inhibitors of fibril formation.

Human lysozyme is a small monomeric enzyme, consisting of 130 residues with four disulfide bonds in its native state structure. Four single-point mutations (I56T, F57I, W64R, and D67H) and two double mutations (F57I/T70N and T70N/W112R) in the protein have been found to be associated with a familial non-neuropathic systemic amyloidosis, which involves the abnormal deposition of the lysozyme variants as insoluble amyloid fibrils in a variety of organs, such as the liver, spleen, and kidneys (*1*−*4*). The effects of the I56T and D67H mutations on the activity, stability, structure, folding, dynamics, and in vitro aggregation of lysozyme have been studied extensively (for reviews, see refs *5*−*7*).

The structure of the native state of lysozyme is composed of two domains; one is largely helical and is denoted the α-domain, while the other domain, termed the β-domain,

† P.-H.C. acknowledges receipt of a scholarship from the Gates Cambridge Trust. M.D. was supported by postdoctoral fellowships from the European Community, the Wellcome Trust, and the Belgian FRS-FNRS. J.C. was supported by the Wellcome Trust and J.R.K. by an NSERC (Canada) postdoctoral fellowship. C.R. was supported by the EPA Cephalosporin Fund and the Wellcome Trust. D.S. is supported by a FWO research fellowship. A.M. is a Research Associate of the Belgian FRS-FNRS and is supported in part by a grant from the Belgian FRFC (Contracts 2.4550.05 and 2.4511.06). C.V.R. is a Royal Society University Research Professor, and the research of C.M.D. is supported in part by Programme Grants from the Wellcome Trust and the Leverhulme Trust. This work was also supported by a BBSRC grant (to C.M.D., C.V.R., and D.B.A.), by the Belgian Programme of Interuniversity Attraction Poles initiated by the Federal Office for Scientific Technical and Cultural Affairs (IAP P5/33 and P6/19), the FWO-Onderzoeksproject, and by the Community's Sixth framework program (Project LSHM-CT-2006-037525). E. D. G. was supported by postdoctoral fellowships from the European Community and EMBO.

* To whom correspondence should be addressed. M.D.: Laboratoire d'Enzymologie, Centre d'Ingénierie des Protéines, Institut de Chimie B6, Université de Liège, B-4000 Liège (Sart Tilman), Belgium; telephone, 003243663546; fax, 003243663364; e-mail, mdumoulin@ulg.ac.be. C.M.D.: Department of Chemistry, University of Cambridge, Lensfield Road, Cambridge CB2 1EW, U.K.; fax, 0044123763418; e-mail, cmd44@cam.ac.uk.

‡ University of Cambridge.
§ Laboratorium voor Ultrastructuur, Vrije Universiteit Brussel.
|| Department of Molecular and Cellular Interactions, VIB, Vrije Universiteit Brussel.
⊥ Université de Liège.
Laboratorium voor Cellulaire en Moleculaire Immunologie, Vrije Universiteit Brussel.
+ University of Nottingham.
○ University of Oxford.

10.1021/bi8005797 CCC: $40.75
Published on Web 09/25/2008

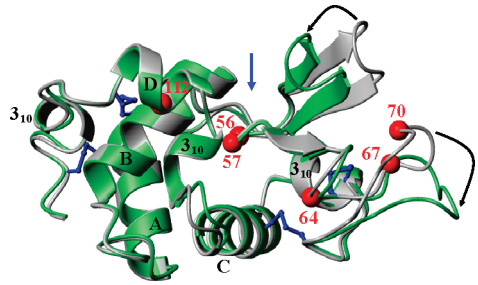

FIGURE 1: Overlay of ribbon diagrams representing the structures of WT-HuL (gray) and the D67H variant (green); the structure of the I56T variant is indistinguishable from that of WT-HuL (*9*). The α-helices are labeled A−D, and the 3_{10}-helices are indicated. The four disulfide bonds are colored blue, and the C_α atoms of residues 56, 57, 64, 67, 70, and 112 are represented as red spheres. The black arrows indicate the relative changes in the positions of residues 42−55 and 66−75 in the D67H variant compared to the wild-type protein. The active site of the protein is located at the back side of the molecule as shown by the blue arrow. The structures of lysozymes were generated from coordinates determined by X-ray diffraction (PDB entries 1LYY, 1LOZ, and 1LZ1) and produced using MOLMOL (*48*).

contains an antiparallel triple-stranded β-sheet, a short 3_{10}-helix, and a long loop (Figure 1) (*8*). The interface between these two domains encompasses the active site of the protein. X-ray crystallographic studies have shown that the native structure of the I56T variant is very similar to that of wild-type human lysozyme (WT-HuL)[1] (*9*). In contrast, in the D67H variant, the two β-strands (residues 42−55) and the long loop (residues 66−75) within the β-domain are significantly distorted due to the disruption by the mutation of the local hydrogen bonding network (*9*) (Figure 1). Although the I56T and D67H variants have been found to be enzymatically active, the D67H protein has significantly reduced activity relative to that of the wild-type protein. This effect results from a combination of a lower substrate binding affinity and a less efficient turnover number (*9*), perhaps resulting from the structural distortions in the active site induced by the movement of the β-domain in this variant protein.

The structures of both the I56T and D67H variants, however, show subtle conformational changes at the interface between the α- and β-domains, which lead to a comparable reduction in the stability of both these variants compared to that of WT-HuL (*9*−*11*). Furthermore, both mutations lead to a significant reduction in the global cooperativity of the protein (*9, 10, 12*). Hydrogen−deuterium (H−D) exchange experiments followed by nuclear magnetic resonance (NMR) spectroscopy and electrospray ionization mass spectrometry (ESI-MS) show that both the I56T and D67H variants, but not the wild-type protein, populate a partially unfolded species under physiologically relevant conditions (*10, 12*).

Despite the different locations of the two mutations, this partially unfolded species is remarkably similar for both variants and results from the region of the protein comprising the β-domain and the adjacent C-helix of the native state being transiently but cooperatively unfolded, whereas the regions forming the remainder of the α-domain maintain their native-like structure (*10, 12*). Taken together, these studies indicate that the reduction in global cooperativity, and the associated ability to populate transiently a specific partially unfolded intermediate state under physiologically relevant conditions, is a common feature underlying the amyloidogenicity of the I56T and D67H proteins (*9, 10, 12*). The formation of intermolecular interactions between the regions that are unfolded in this intermediate state [i.e., the β-domain and the C-helix that we denote as the "amylotope" (Figure 4B)] is therefore likely to be a fundamental trigger of the aggregation process that ultimately leads to the formation and deposition of amyloid fibrils in tissue (*9, 10, 12*).

Human lysozyme is therefore a prototypic example of how a reduction in stability and global cooperativity correlates with the propensity of a protein to aggregate into amyloid fibrils. One possible strategy for inhibiting the aggregation process of such a protein is to enhance its stability via, for example, the binding of a small molecule. We have previously demonstrated that binding cAb-HuL6, the antigen-binding domain of a heavy-chain antibody (HCAb) specific for human lysozyme, to both the I56T and D67H variant proteins does restore the stability and the high degree of cooperativity that is characteristic of the wild-type lysozyme and, as a result, inhibits dramatically the in vitro formation of fibrils by both variants (*10, 13*). Structural studies of the complex between cAb-HuL6 and lysozyme reveal that the antibody fragment acts through a subtle mechanism involving only 11 of the nearly 60 residues participating in the transient unfolding of the I56T and D67H variants. The effects of the binding of cAb-HuL6 are therefore not simply to mask the entire region of the protein destabilized by the mutations; rather, it appears that cAb-HuL6 restores the global cooperativity through long-range conformational effects at the interface between the two structural domains of lysozyme (*10, 13*). These results encouraged us to generate other antigen-binding domains of HCAbs, which are termed V_HHs (*14*) or nanobodies (*15*), directed against different epitopes on human lysozyme and to study how their binding perturbs the stability, cooperativity, and aggregation propensity of the lysozyme variants.

In this study, we selected a nanobody, cAb-HuL22, that binds to the active site of human lysozyme and we engineered a variant of it (cAb-HuL22-S54C/I78C) containing an extra disulfide bridge and that is functional under the conditions used to form lysozyme fibrils in vitro. We report a detailed analysis of the effects of binding of cAb-HuL22 on the stability, cooperativity, and aggregation propensity of the I56T and D67H variants of human lysozyme, using a variety of techniques, including optical spectroscopic methods, and H−D exchange experiments analyzed by ESI-MS and NMR. As mentioned above, the I56T and D67H proteins behave very similarly, and therefore, the effects of cAb-HuL22

[1] Abbreviations: ANS, 8-anilino-1-naphthalenesulfonic acid; cAb-HuL22, variable domain of a camelid heavy-chain antibody raised against wild-type human lysozyme; cAb-HuL22-S54C/I78C, variant of cAb-HuL22 in which the S54C and I78C mutations have been introduced; CDRs, complementary determining regions; EM, electron microscopy; ESI-MS, electrospray ionization mass spectrometry; $(GlcNAc)_3$, *N*,*N*′,*N*″-triacetylchitotriose; H−D exchange, hydrogen−deuterium exchange; HCAb, heavy-chain antibody; HSQC, heteronuclear single-quantum coherence; IC_{50}, concentration of inhibitor that reduces the lysozyme activity by 50%; ITC, isothermal titration calorimetry; k_a, kinetic rate constant for association; k_d, kinetic rate constant for dissociation; K_D, equilibrium dissociation constant; NMR, nuclear magnetic resonance; NOESY, nuclear Overhauser effect spectroscopy; SPR, surface plasmon resonance; T_m, temperature of midtransition; Thio-T, thioflavin T; UV CD, ultraviolet circular dichroism; V_HH, variable domain of a camelid heavy-chain antibody; WT-HuL, wild-type human lysozyme.

binding on their properties were in same cases explored by studying only one of the two variants. The results of this study show that cAb-HuL22 stabilizes the native state of the lysozyme variants upon binding in the enzyme active site and, as a consequence, inhibits the formation of amyloid fibrils. These findings support the premise that the reduction in cooperativity of the amyloidogenic variants is at the origin of their amyloidogenicity. They also suggest a possible therapeutic strategy for limiting the effects of genetic mutations in patients, and they emphasize further the value of single-domain camelid antibody fragments in dissecting and interfering with the mechanism of amyloid fibril formation.

MATERIALS AND METHODS

Generation and Selection of cAb-HuL22 and cAb-HuL22-S54C/I78C. A wild-type human lysozyme preparation was used for dromedary immunization, as described previously (*16*). A phage library containing the genes encoding the variable domains of the heavy-chain antibodies was generated using the mRNA extracted from the lymphocytes of the immunized dromedary (*17*). A V_HH specific for human lysozyme, denoted cAb-HuL22, were isolated by biopanning from this phage library. The S54C/I78C variant of cAb-HuL22 (denoted cAb-HuL22-S54C/I78C) was generated as described previously (*18*).

Proteins. Wild-type human lysozyme, including uniformly ^{15}N-labeled protein, was expressed in *Pichia pastoris* and purified as described previously (*19*). The I56T and D67H lysozyme variants, including uniformly ^{15}N-labeled protein, were expressed in *Aspergillus niger* and purified following established protocols (*20*). cAb-HuL22 and cAb-HuL22-S54C/I78C were expressed in *Escherichia coli* and purified to homogeneity as described previously (*21*). The affinities of the antibody fragments for the various lysozyme species were determined using surface plasmon resonance following the protocol described previously (*21*). The protein concentrations were determined on the basis of $A^{1\%}_{280}$ values of 2.55, 2.00, and 2.00 for lysozyme, cAb-HuL22, and cAb-HuL22-S54C/I78C, respectively.

Competitive Binding of cAb-HuL22 and $(GlcNAc)_3$ to WT-HuL. The kinetics of binding of cAb-HuL22 to WT-HuL in the presence of increasing concentrations of *N*,*N*′,*N*″-triacetylchitotriose [$(GlcNAc)_3$] were analyzed by SPR spectroscopy using a Biacore 2000 instrument. Approximately 260 RU of WT-HuL was immobilized on a CM5 sensor chip using amine coupling chemistry (EDC/NHS) according to the manufacturer's instructions. α-Lactalbumin was used as a reference; hence, baseline sensorgrams could be obtained to allow subtraction of bulk refractive index background. Binding traces of a series of solutions of cAb-HuL22 (500 nM) containing different concentrations of the inhibitor $(GlcNAc)_3$ (0, 80, 159, 319, 797, 1593, and 2390 μM) in 10 mM HBS-EP buffer [10 mM HEPES, 3 mM EDTA, 0.005% (v/v) surfactant P20, and 150 mM NaCl (pH 7.4)] were recorded. The SPR signals for the binding of WT-HuL to these solutions were monitored at a flow rate of 30 μL/min at 25 °C; under these conditions, the mass transfer effects proved to be negligible.

Inhibition of Lysozyme Activity by cAb-HuL22 and cAb-HuL22-S54C/I78C. The inhibitory capacity of cAb-HuL22 and cAb-HuL22-S54C/I78C was determined by preincubating lysozyme (150 μL of 80 nM WT-HuL or D67H variant solutions) with various concentrations of antibody fragment for at least 15 min at 25 or 45 °C in a 96-well plate. After the addition of 50 μL of *Micrococcus lysodeikticus* (180 μg/mL, previously incubated at the appropriate temperature), the initial rate of hydrolysis was measured as a decrease in absorbance at 450 nm using a Spectra max 340 plate reader (Molecular Devices). The 50% inhibitory concentrations (IC_{50}) were obtained by plotting lysozyme residual activity as a function of increasing antibody fragment concentration. The measurements were carried out in 0.1 M citrate buffer (pH 5.5) at 25 °C and in 0.1 M citrate buffer (pH 5.5) containing 3 M urea at 45 °C (which was the upper temperature limit of the plate reader). The IC_{50} for $(GlcNAc)_3$ was also measured for comparison. A minimum of 10 replicates per measurement were performed for each antibody fragment concentration, and two independent series of measurements were conducted for each condition (except for measurements carried out at 45 °C).

Measurement of the Affinity of cAb-HuL22-S54C/I78C for WT-HuL under Fibril-Forming Conditions. The interaction of cAb-HuL22-S54C/I78C with WT-HuL was assessed by isothermal titration calorimetry (ITC) using a VP-ITC instrument (MicroCal Inc.) with a cell volume of 1.4227 mL. The assay was performed at 48 °C in 0.1 M citrate buffer (pH 5.5) containing 3 M urea. Lyophilized cAb-HuL22-S54C/I78C and WT-HuL were dissolved in 0.1 M citrate buffer (pH 5.5) containing 3 M urea and run on a Superdex 75 10/30 gel filtration column, previously equilibrated with the same buffer, to ensure a matching buffer composition and to remove any protein aggregates. Fractions corresponding to monomeric proteins were then pooled and degassed. cAb-HuL22-S54C/I78C was loaded into the ITC cell, and WT-HuL was loaded into the syringe. The concentrations of WT-HuL and cAb-HuL-S54C/I78C were 308 and 34 μM, respectively. A 4 μL injection was followed by 27 injections of 10 μL of WT-HuL, and the measurements were done in duplicate. After baseline correction, the heats for each injection were integrated and plotted versus the molar ratio of HuL to cAb-HuL22-S54C/I78C. Correction factors for the heat of dilution and mixing were obtained by manual subtraction of the heat at saturation of binding. Data were processed using MicroCal Origin 7.0. According to the manufacturer's recommendations, the integrated heat of the 4 μL injection was discarded for further analysis due to the large inaccuracy of the measured heat for the initial injection due to diffusion and leakage effects. The observed binding dissociation constants were obtained from a nonlinear least-squares fit to a 1:1 binding model provided by MicroCal Origin 7.0.

Aggregation Monitored by Absorbance Measurements at 600 nm. Stock solutions of proteins were prepared from lyophilized material, passed through a 0.22 μm filter, diluted to the desired final concentration in 0.1 M citrate buffer (pH 5.5) containing 3 M urea, and incubated at 48 °C, while being stirred in a Uvikon XS spectrophotometer equipped with a 12-cell Peltier holder. The final lysozyme concentration was 6.8 μM, and the final concentration of the V_HH was between 0 and 34 μM. Protein aggregation was monitored through changes in absorbance measured at 600 nm.

Heat-Induced Unfolding Monitored by Far-UV CD. Heat-induced unfolding transitions were monitored by far-UV CD

using a Jasco J-810 spectropolarimeter equipped with a six-cell Peltier holder with a 0.1 cm path lengh cell. The lysozyme and V_HH concentrations were 14 μM in 0.1 M citrate buffer (pH 5.5) containing 3 M urea. The temperature was increased monotonically from 25 to 97 °C at a rate of 0.5 °C/min and was monitored throughout the experiment using a thermocouple. Mineral oil was added to the top of the samples to limit evaporation. Data were acquired every 1 °C, with a 2 s integration time and a 2 nm bandwidth. The unfolding curves were analyzed assuming a two-state unfolding model (*22*).

Pulse Labeling Hydrogen−Deuterium Exchange of the Variants Analyzed by Mass Spectrometry. The I56T and D67H human lysozyme variants were deuterated at exchangeable sites by unfolding the proteins in deuterated guanidinium hydrochloride (predeuterated by three cycles of dissolution in ^2H_2O, followed by lyophilization), and subsequent refolding in deuterated buffer [50 mM deuterated acetic acid (pH* 5.0)]. The proteins were subsequently concentrated using Centriprep-3 concentrators (Amicon, Millipore), and the buffer was changed to ^2H_2O by consecutive cycles of dilution and concentration in ^2H_2O, until no guanidinium ion contamination was observed in the mass spectra. The final concentration of lysozyme was 8 μM. For the experiments carried out in the presence of the cAb-HuL22 fragment, the deuterated I56T (or D67H) variant and the protonated cAb-HuL22 fragment were mixed immediately prior to the experiment to give a ratio of I56T (or D67H) to cAb-HuL22 of 1:2 (to ensure essentially all the lysozyme molecules were in the nanobody-bound state) before H−D exchange experiments were performed. We prepared pulse-labeled samples by manually mixing 20 μL of the protein solution with 300 μL of pulse labeling buffer (100 mM ammonia/formic acid in H_2O at pH 8 at 37 °C). The exchange was allowed to proceed for various periods of time ranging between 5 and 300 s. The resulting protein solutions were then mixed with 140 μL of 1 M acetic acid in H_2O to generate a final pH of 3.5 for the solutions. After quenching, the samples were stored on ice before being analyzed by mass spectrometry. A fully exchanged sample was prepared by incubating proteins in pulse labeling buffer for 15 min at 80 °C prior to quenching. The samples were electrosprayed at the base pressure of a LC-ToF spectrometer (Micromass), with a cone voltage of 80 V. No adjustments to the total number of exchanged proton atoms for the 6% deuterium present in the pulse solution were made. Mass spectra shown in Figure 6 represent the convolution of the +8, +9, and +10 charge states with minimal smoothing and were converted to a mass scale.

NMR Studies of the WT-HuL−cAb-HuL22 Complex. An NMR sample of the complex was made up and contained ~1.2 mM unlabeled cAb-HuL22 and ~0.6 mM ^{15}N-labeled WT-HuL at pH 6.5 in 20 mM phosphate buffer made up with a 95% H_2O/5% ^2H_2O mixture. The excess antibody concentration ensured that all the lysozyme molecules were bound to an antibody molecule in the complex. Two-dimensional ^{15}N−^{1}H HSQC spectra of WT-HuL in the presence and absence of the unlabeled cAb-HuL22 fragment were recorded at 35 °C using a Bruker Biospin Avance 700 NMR spectrometer equipped with a cryo-platform. The HSQC spectra were collected with 2048 and 256 complex points in t_1 (^{1}H) and t_2 (^{15}N), respectively, with sweep widths of 8389 and 2483 Hz in the ^{1}H and ^{15}N dimensions, respectively. The ^{1}H and ^{15}N resonances of WT-HuL in complex with cAb-HuL22 were assigned by ^{15}N-edited three-dimensional (3D) NOESY-HSQC measurements. These spectra were collected with 138, 74, and 2048 complex points in t_1 (^{1}H), t_2 (^{15}N), and t_3 (^{1}H), respectively. The observed NOE data for the antibody−lysozyme complex were interpreted by using the assignments of the free lysozyme (*23*). All the NMR spectra were processed with NMRPipe and Sparky (http://www.cgl.ucsf.edu/home/sparky/).

NMR Studies of the Hen Lysozyme−cAb-Lys3 Complex. An NMR sample of the complex was made up and contained ~0.7 mM unlabeled cAb-Lys3 and ~0.6 mM ^{15}N-labeled hen lysozyme at pH 6.5 in 20 mM phosphate buffer made up with a 95% H_2O/5% ^2H_2O mixture. The excess of nanobody ensured that all the lysozyme molecules were bound to an antibody fragment molecule in the complex. A two-dimensional (2D) ^{15}N−^{1}H HSQC spectrum of the hen lysozyme bound to the nanobody was collected at 35 °C on a 750 MHz spectrometer. The spectrum was collected with 128 complex t_1 increments of 64 transients and 1024 complex data points. Sweep widths of 10582 and 2273 Hz were used in the F_2 and F_1 dimensions, respectively. The data were processed with a Gaussian window function in F_2 and a 90°-shifted sine bell in F_1, using FELIX (Accelrys). After zero-filling, the digital resolution was 5.2 and 4.4 Hz/point in F_2 and F_1, respectively. The ^{1}H and ^{15}N resonances of hen lysozyme in complex with cAb-Lys3 were assigned using ^{15}N-edited 3D NOESY-HSQC experiments. These spectra were collected with 128, 30, and 512 complex points in t_1 (^{1}H), t_2 (^{15}N), and t_3 (^{1}H), respectively. The observed NOE data for bound hen lysozyme were interpreted by using published assignments for the free protein (*24, 25*).

Electron Microscopy. Samples were applied to Formvar-coated nickel grids, stained with a 2% (w/v) uranyl acetate solution, and viewed in a Phillips CEM100 transmission electron microscope operating at 80 kV.

Thioflavin T. A stock of thioflavin T (Thio-T) (2.5 mM) was prepared in 10 mM sodium phosphate buffer (pH 7.0) containing 150 mM NaCl (Thio-T buffer), passed through a 0.22 μm pore size filter, and stored at −20 °C. On the day of the experiment, an aliquot of the Thio-T stock was thawed and diluted to a final concentration of 50 μM in Thio-T buffer to make the Thio-T working solution. Fifty microliters of the protein sample were added to 1500 μL of Thio-T working solution in a 1 cm path length cuvette. Thio-T fluorescence was measured with a Perkin-Elmer LS50B spectrofluorimeter. The excitation wavelength was 440 nm; the emission spectra were recorded between 450 and 600 nm, and the excitation and emission slit widths were 5 nm. Twenty-five scans were averaged at a scan speed of 600 nm/min at room temperature. The spectra were corrected for the background fluorescence of a solution of Thio-T.

RESULTS

cAb-HuL22 Binds in the Active Site of Human Lysozyme. Among the nanobodies with specificity for human lysozyme that have been selected from a library of V_HH genes cloned from the blood of a dromedary immunized with WT-HuL, cAb-HuL22 seemed particularly interesting and was therefore chosen for detailed characterization for two reasons. First,

Table 1: Kinetic Rate Constants for Association (k_a) and Dissociation (k_d) and Equilibrium Dissociation Constants (K_D) of cAb-HuL22− and cAb-HuL22-S54C/I78C−Lysozyme Complexes Determined by SPR Spectroscopy and ITC[a]

	WT-HuL	I56T	D67H
	cAb-HuL22		
k_a[b] (M^{-1} s^{-1})	3.3×10^5	3.1×10^5	2.3×10^5
k_d[b] (s^{-1})	11.3×10^{-3}	10.5×10^{-3}	34.2×10^{-3}
K_D[b] (nM)	35	34	150
IC_{50}[c] (nM)	106 ± 12	Nd[f]	Nd[f]
	cAb-HuL22-S54C/I78C		
k_a[b] (M^{-1} s^{-1})	2.7×10^5	2.8×10^5	2.0×10^5
k_d[b] (s^{-1})	13.4×10^{-3}	13.0×10^{-3}	43.0×10^{-3}
K_D[b] (nM)	50	47	220
K_D[d] (nM)	940 ± 120	Nd[f]	Nd[f]
IC_{50}[c] (nM)	139 ± 11	Nd[f]	615 ± 110
IC_{50}[e] (nM)	4700	Nd[f]	21000

[a] The antibody fragment concentration inhibiting 50% of the lysozyme activity (IC_{50}) is also indicated. [b] Determined at 25 °C in 10 mM HEPES buffer (pH 7.5) by SPR spectroscopy. The standard deviations are <20%. [c] Determined at 25 °C in 0.1 M citrate buffer (pH 5.5). [d] Determined at 48 °C in 0.1 M citrate buffer (pH 5.5) containing 3 M urea by ITC measurements. [e] Determined at 45 °C in 0.1 M citrate buffer (pH 5.5) containing 3 M urea. [f] Not determined.

SPR measurements show that cAb-HuL22 and cAb-HuL6 can bind simultaneously to WT-HuL, suggesting that the two V_HHs recognize different epitopes (data not shown). More importantly, the affinity of cAb-HuL22 for the D67H variant (K_D = 150 nM) was ~5 times lower than that for I56T (K_D = 34 nM) and wild-type lysozyme (K_D = 35 nM) (Table 1). This observation suggests that Asp67 is directly involved in the recognition and/or binding of cAb-HuL22 or that this antibody fragment recognizes a region of the protein structure that is different in the D67H variant from that of the WT-HuL and I56T structures [i.e., the β-strands (residues 42−55) or the long loop (residues 66−75) within the β-domain (Figure 1) (*9*)]. As previously mentioned, this region encompasses part of the enzyme binding site, and cAb-HuL22 could therefore be an inhibitor of the enzyme.

Competitive binding between cAb-HuL22 and *N*,*N*′,*N*″-triacetylchitotriose $(GlcNAc)_3$, a substrate analogue that binds reversibly to the enzyme (*26*), was investigated by SPR experiments. Because $(GlcNAc)_3$ binds weakly to WT-HuL (K_D = 38 μM) (*26*) relative to the cAb-HuL22 fragment (K_D = 35 nM), its concentrations were set in a range (0.08−2.39 mM) that permits effective competition with the cAb-HuL22 fragment (500 nM). Figure 2A shows the SPR signals for the cAb-HuL22−WT-HuL complex in the absence and presence of different concentrations of $(GlcNAc)_3$. The level of binding of cAb-HuL22 decreases substantially as the concentration of $(GlcNAc)_3$ increases, indicating that the fragment is a competitive inhibitor of the enzyme and thus binds in the active site of the protein. The inhibitory capacity of cAb-HuL22 was estimated from the initial rate of *M. lysodeikticus* hydrolysis by WT-HuL (80 nM) in the presence of different concentrations of the antibody fragment (Figure 2B), and the concentration of antibody fragment that inhibits 50% of the activity (IC_{50}) was determined. The IC_{50} value obtained for cAb-HuL22 is 106 ± 12 nM; it is in the same range as the enzyme concentration. Under the same conditions, the IC_{50} measured for $(GlcNAc)_3$ is ~600-fold higher (i.e., 65 ± 10 μM). This result indicates that cAb-HuL22 acts as a very good inhibitor of lysozyme activity.

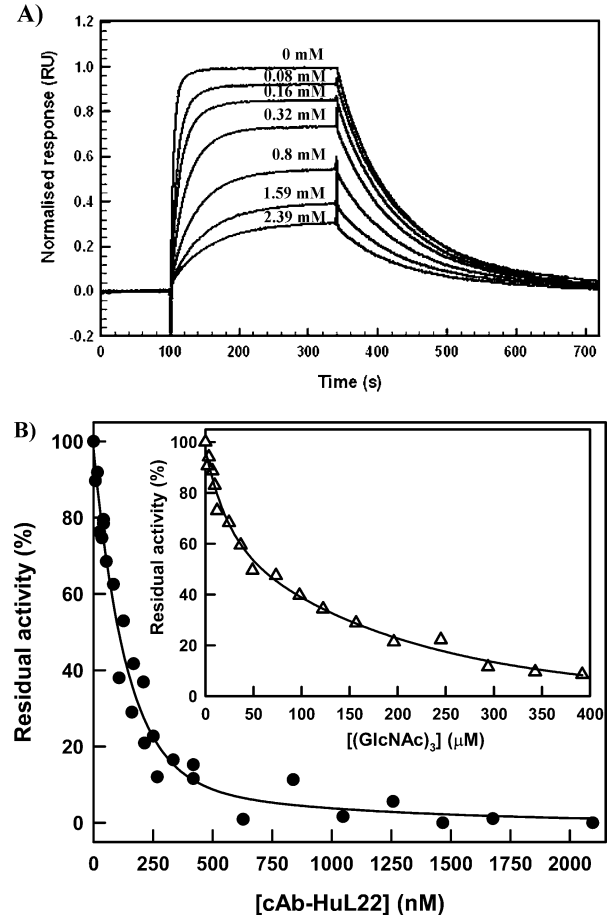

FIGURE 2: cAb-HuL22 is a competitive inhibitor of HuL. (A) Competitive binding between cAb-HuL22 and $(GlcNAc)_3$ monitored by SPR. Sensorgrams for the binding of the cAb-HuL22 fragment (500 nM) to WT-HuL were recorded in the presence of different concentrations from 0 to 2.39 mM of the inhibitor $(GlcNAc)_3$. The SPR signals were recorded at 25 °C in 10 mM HBS-EP buffer at a flow rate of 30 μL/min at 25 °C. (B) Inhibition of lysozyme activity by cAb-HuL22 and $(GlcNAc)_3$ (inset). The residual hydrolytic activity of lysozyme in the presence of various concentrations of cAb-HuL22 and $(GlcNAc)_3$ is plotted relative to that measured in their absence. The measurements were carried out in 0.1 M citrate buffer (pH 5.5) at 25 °C.

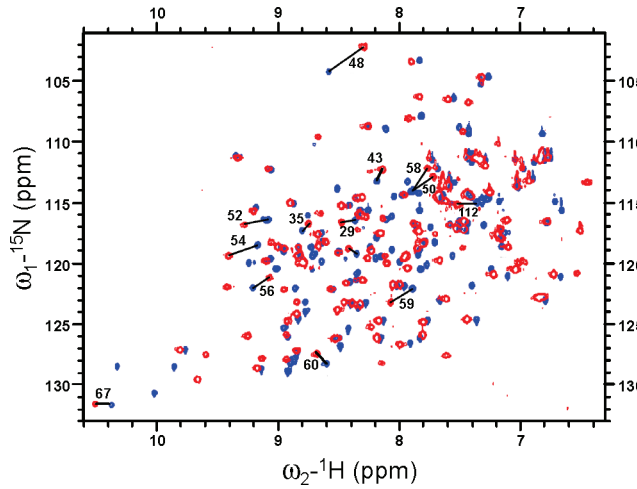

FIGURE 3: Mapping the binding site of cAb-HuL22 on WT-HuL by NMR spectroscopy. Overlaid $^{15}N-^{1}H$ HSQC NMR spectra at 700 MHz of WT-HuL with (red) and without (blue) the cAb-HuL22 fragment. The spectra were recorded at pH 6.5 and 35 °C.

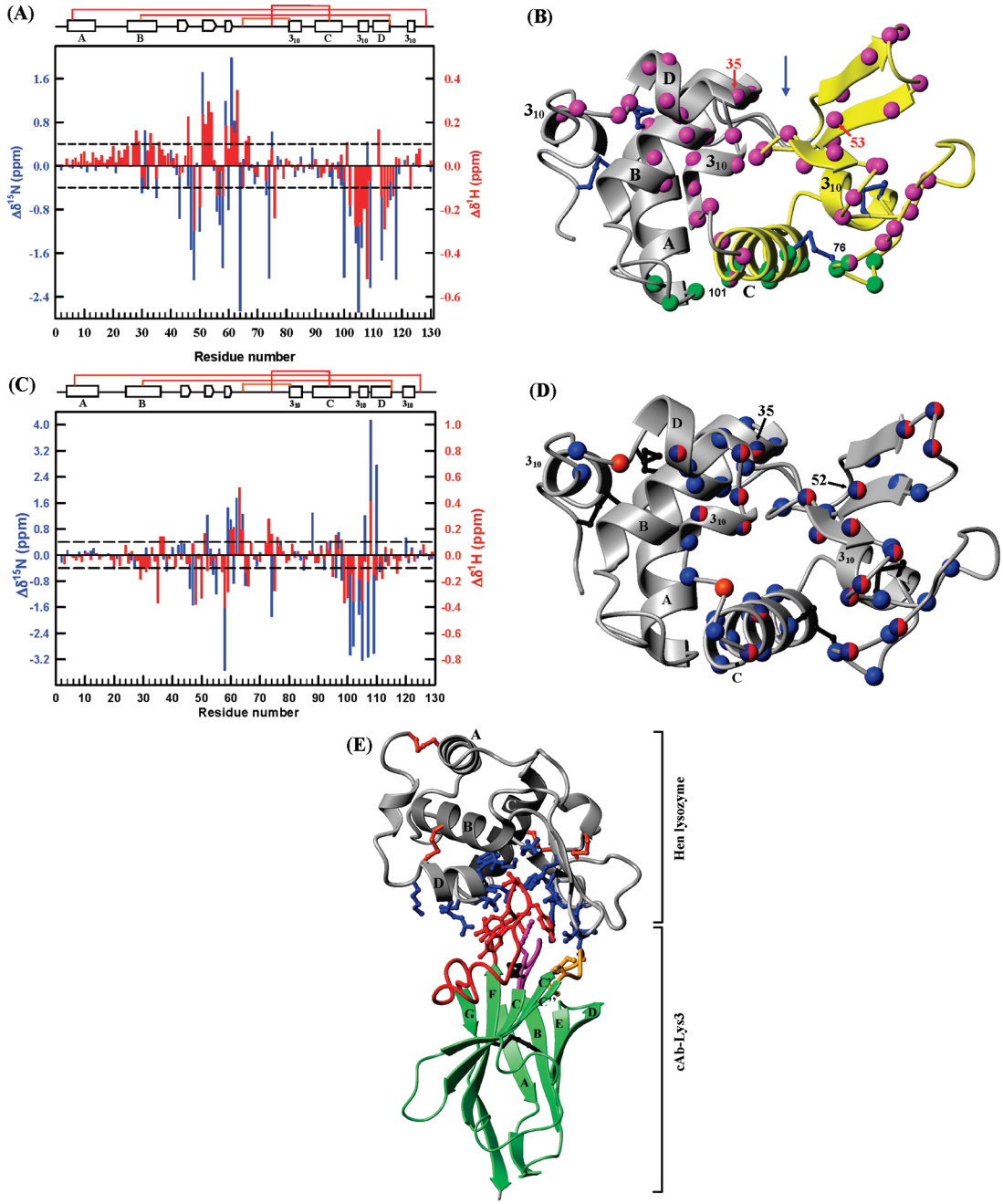

FIGURE 4: Mapping the binding site of cAb-HuL22 on HuL and of cAb-Lys 3 on hen lysozyme by NMR spectroscopy. (A) Chemical shift perturbations induced by the binding of the cAb-HuL22 fragment to WT-HuL. The blue and red bars represent the chemical shift perturbations of the ^{15}N and ^{1}H resonances, respectively. Residues experiencing a chemical shift change of $\geq|0.4|$ ppm for ^{15}N or $\geq|0.1|$ ppm for ^{1}H resonances are considered to be affected significantly by the binding of the antibody fragment. (B) Ribbon diagram of WT-HuL showing in magenta space-filling representation the C_α atoms of the residues that are affected significantly by the binding of the cAb-HuL22 fragment. The α-helices are labeled A−D, and the 3_{10}-helices are indicated. The active site of the protein is denoted with the arrow. The four disulfide bonds are colored blue. Note that the catalytic residues, Glu35 and Asp53, which are located deep in the active site exhibit significant chemical shift perturbations. For comparison, residues that have been found in contact with the cAb-HuL6 fragment by X-ray crystallography are colored green (*13*). Residues that are in contact with cAb-HuL6 and whose chemical shift is affected by the binding of cAb-HuL22 are colored half-magenta and half-green (i.e., residues 76 and 101). The amylotope (i.e., the region of the molecule that unfolds transiently in a locally cooperative manner) is colored yellow. The human lysozyme structure was generated from its X-ray coordinates (PDB entry 1LZ1) and produced using MOLMOL (*48*). (C) Chemical shift perturbations by the binding of the cAb-Lys3 fragment to hen lysozyme. The blue and red bars represent the chemical shift perturbations of the ^{15}N and ^{1}H resonances, respectively. Residues experiencing a chemical shift change of $\geq|0.4|$ ppm for ^{15}N or $\geq|0.1|$ ppm for ^{1}H resonances are considered to be affected significantly by the binding of the antibody fragment. (D) Ribbon diagram of hen lysozyme showing the C_α atoms of the residues affected significantly by the binding of the cAb-Lys3 fragment in a blue space-filling representation. Note that the catalytic residues, Glu35 and Asp52, are spatially closely similar to Glu35 and Asp53, respectively, of WT-HuL. Residues found to be in direct contact with cAb-Lys3 are colored red. Residues that both show significant chemical shift perturbations (this work) and are directly involved in the binding to the cAb-Lys3 fragment (X-ray crystallography data) (*29*) are colored half-blue and half-red. The structure of hen lysozyme was generated from its X-ray coordinates (PDB entry 2VB1) and produced using MOLMOL (*48*). (E) Ribbon representation of the X-ray structure of hen lysozyme (gray) in complex with cAb-Lys3 (green). The helices of lysozyme and β-strands of cAb-Lys3 are labeled, and the disulfide bridges are colored black and orange in cAb-Lys3 and hen lysozyme, respectively. CDR1, CDR2, and CDR3 are colored magenta, yellow, and red, respectively. The long CDR3 (26 residues) inserts deeply into the active site. The side chains of residues constituting the epitope are colored blue; those constituting the paratope are colored red (from CDR3), magenta (from CDR1) and yellow (from CDR2). The structure of the complex was generated from its X-ray coordinates (PDB entry 1MEL) and produced using MOLMOL (*48*).

We previously showed that the binding region of a V_HH on the lysozyme structure can be probed in a specific manner by analysis of the chemical shift perturbations of the resonances of the amide groups of individual amino acid residues (*10, 13*). To investigate the interactions of the cAb-HuL22 fragment with human lysozyme at the molecular level, we compared the $^{15}N-^{1}H$ HSQC NMR spectrum of free WT-HuL, uniformly labeled with ^{15}N, with that of the ^{15}N-labeled protein in complex with the unlabeled antibody fragment (Figure 3). Detailed analysis of the spectra reveals that 49 residues of WT-HuL exhibit significant chemical shift perturbations ($|\Delta\delta^{1}H| \geq 0.1$ ppm or $|\Delta\delta^{15}N| \geq 0.4$ ppm) upon binding to the cAb-HuL22 fragment (Figure 4A). These residues are located primarily in the B- and D-helices, in the 3_{10}-helix following the C-helix within the α-domain, and in the *β*-strands and long loop within the *β*-domain (Figure 4B).

It is interesting to note that 13 of the 49 residues affected by the binding of cAb-HuL22 are located in regions of the *β*-domain (residues 42−55 and 66−75) that are distorted in the D67H variant (Figures 1 and 4B) (*9*). This observation is in good agreement with the findings from the SPR studies that the binding affinity of cAb-HuL22 for the D67H variant is lower than for the I56T and WT-HuL lysozymes (Table 1). Furthermore, the region containing the residues that exhibit significant chemical shift perturbations on binding the antibody fragment encompasses much of the active site (*27*), including the catalytically important residues (Glu35 and Asp53), which is located at the interface between the α- and *β*-domains (Figure 4B). This observation, therefore, strongly suggests that the cAb-HuL22 fragment interacts with a number of residues in the active site of human lysozyme.

cAb-Lys3 is a V_HH specific to hen lysozyme, a protein closely similar to WT-HuL in sequence (the two enzymes are 60% identical in sequence) and structure (*8, 28*), that binds in the active site of the enzyme, as shown by X-ray crystallography (*29*). Comparison of the chemical shift perturbations induced by the binding of cAb-HuL22 to WT-HuL with those induced by the binding of cAb-Lys3 to hen lysozyme could therefore provide further information about the binding site of cAb-HuL22. The analysis of the chemical shift perturbations shows that 53 residues of hen lysozyme exhibit significant chemical shift perturbations ($|\Delta\delta^{1}H| \geq 0.1$ ppm or $|\Delta\delta^{15}N| \geq 0.4$ ppm) upon binding to the cAb-Lys3 fragment (Figure 4C); this number is similar to that observed for the binding of cAb-HuL22 on WT-HuL (i.e., 49). These residues include most of those that have been found to be in direct contact with the antibody fragment in the crystal structure (Figure 4D) (*29*). The locations in the structure of hen lysozyme of the residues whose chemical shifts are affected by the binding of cAb-Lys3 are remarkably similar to the locations of those in WT-HuL affected by the binding of cAb-HuL22 (Figure 4B,D). Taken together, these data suggest very strongly that the cAb-HuL22 fragment binds in the active site of human lysozyme, in a manner similar to that of the binding of cAb-Lys3 to hen lysozyme (Figure 4E).

The cAb-HuL22 and cAb-Lys3 fragments exhibit remarkably similar structural features. The two V_HHs each display a long CDR3 loop, consisting of 29 and 26 residues, respectively (Figure 5), far above the typical value of 16−18 residues observed with most V_HHs (*14*). The X-ray crystallography structure of the complex between cAb-Lys3 and hen lysozyme (Figure 4E) reveals that the long CDR3 loop extends deep into the active site of the enzyme (*29*). Moreover, the CDR3 loops of both V_HHs contain a disulfide bridge. In cAb-Lys3, this disulfide bridge (C34−C111.6, IMGT numbering) links the long CDR3 to CDR1, whereas in cAb-HuL22, it tethers CDR3 with a framework amino acid at position 50 which is located on framework 2 (C50−C112.6, IMGT numbering); a disulfide bridge between these latter positions has been previously reported for another nanobody (*30*). In the case of cAb-Lys3, it was proposed that this disulfide bridge imposes conformational restraints on the flexibility of the CDR3 loop in the absence of the protein antigen (*29, 31*). Altogether, these results suggest that cAb-HuL22 binds in the active site of human lysozyme via its very long CDR3.

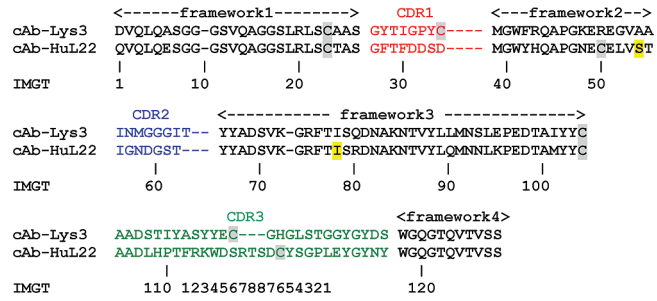

FIGURE 5: Amino acid sequence alignment of cAb-HuL22 and cAb-Lys3. The CDRs and the amino acid are numbered (bottom line) according to the IMGT system (http://imgt.cines.fr). The four cysteines are shaded in gray for both fragments. Positions at which an additional disulfide bond has been engineered in cAb-HuL22 are highlighted in yellow. The CDR3 loop of cAb-HuL22 (29 residues) is by far the longest yet observed for any nanobody.

cAb-HuL22 Restores the Wild-Type Global Cooperativity of the I56T and D67H Variants. The effects of binding of the cAb-HuL22 fragment on the dynamics and structural cooperativity of the I56T and D67H variants were investigated by pulse labeling H−D exchange experiments, monitored by ESI-MS. In these experiments, the labile hydrogen atoms of the lysozyme variants were first fully replaced with deuterium atoms; therefore, the exchange process generated by the pulse dilution into ammonia/formic acid buffer prepared in H_2O led to the replacement of all accessible labile deuterium atoms with hydrogen atoms (see Materials and Methods) (*12*). The pulse exchange reaction was carried out under conditions (pH 8.0 and 37 °C) for which the intrinsic rate of H−D exchange is very high, hence ensuring that effectively all the labile deuterium atoms that are exposed to the solvent will undergo instantaneously simultaneous and irreversible exchange. Spectra of samples pulse labeled for lengths of time ranging from 5 to 300 s, in the presence or absence of cAb-HuL22, are shown in Figure 6.

In the absence of the cAb-HuL22 fragment, the mass spectra of both the I56T and D67H variants show bimodal distributions of peaks as the exchange takes place (Figure 6A,C). The peaks with lower masses (colored yellow) indicate that a cooperative unfolding of a significant region of the proteins occurs during the course of the experiment. This bimodal distribution of masses is consistent with previous results (*10, 12, 13*) and demonstrates that under physiologically relevant conditions, both lysozyme variants populate an intermediate species in which the *β*-domain and

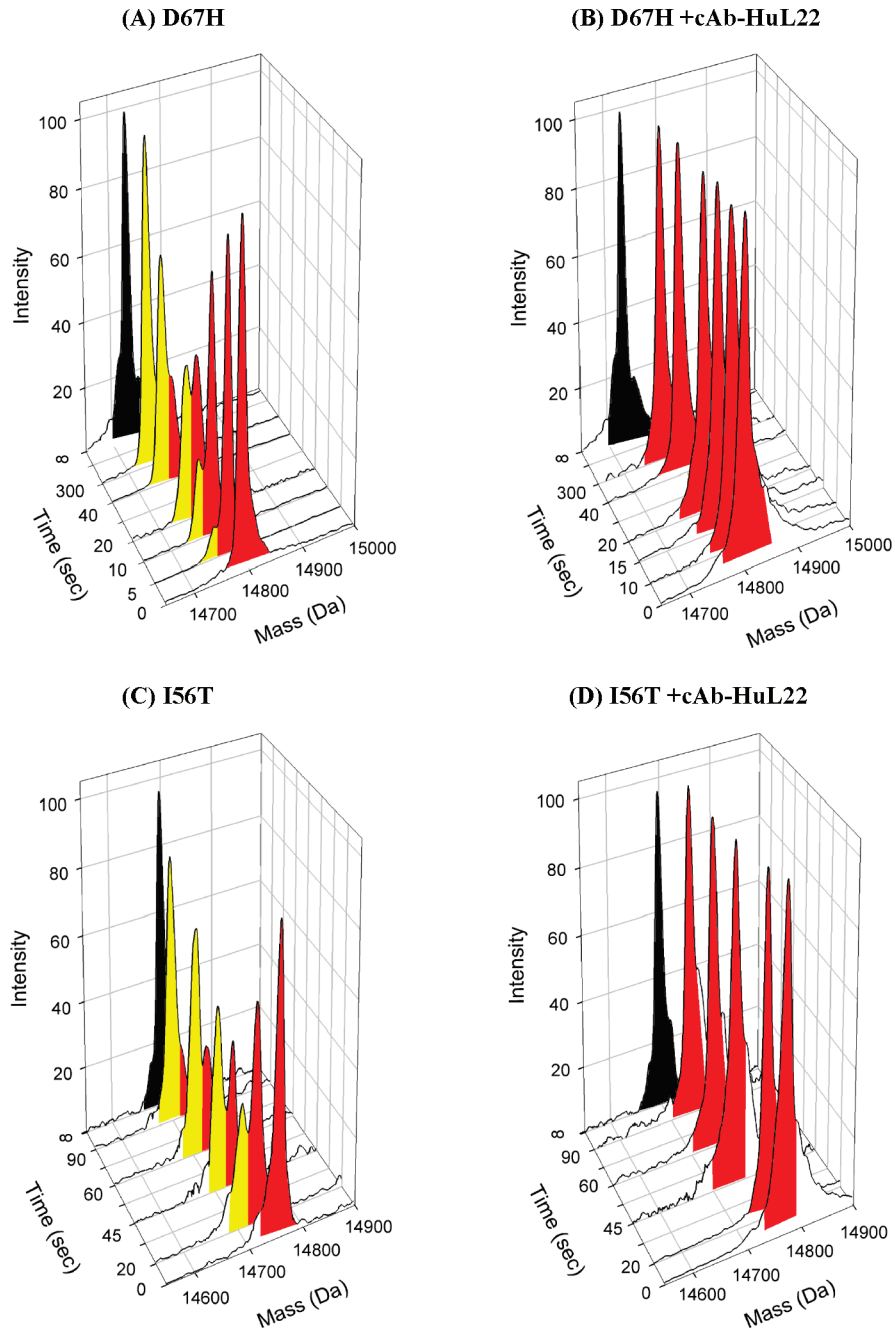

FIGURE 6: Detection of the transient unfolding intermediate of lysozyme in the presence and absence of cAb-HuL22. Electrospray mass spectra of the D67H and I56T variants subjected to H−D exchange in the absence (A and C) and presence (B and D) of a 2-fold excess of the cAb-HuL22 fragment. The peaks observed in spectra of control samples recorded after complete H−D exchange are colored black. The peaks colored red arise from the exchange of deuterium atoms through localized structural fluctuations, whereas those colored yellow arise from the cooperative unfolding of the amylotope. These latter peaks are not observed in the mass spectra of the I56T and D67H variants in the presence of the cAb-HuL22 fragment, indicating that the binding of cAb-HuL22 restores the global cooperativity of the lysozyme variants.

the adjacent C-helix are cooperatively unfolded, albeit transiently, whereas the regions forming the remainder of the α-domain maintain their native-like structure (*10, 12, 13*). The masses of peaks (colored red) decrease slowly with the length of time the exchange was allowed to take place; this behavior has been shown to result from amide deuterium atoms undergoing exchange through localized fluctuations that expose a few amide groups to the solvent at any one time (*12, 13*).

In the presence of the cAb-HuL22 fragment, however, peaks that are observed at lower masses in the absence of the antibody fragment are not seen in the spectra of both the I56T and D67H variants (Figure 6B,D); instead, both variants give rise to a single peak whose mass progressively decreases with time. A similar single set of peaks has been observed with WT-HuL under similar conditions and is characteristic of H−D exchange occurring via local fluctuations occurring independently of each other and involving only a few residues at any one time (*12, 13*). These results demonstrate that in the presence of the antibody fragment, virtually none of the molecules of the variant lysozymes undergo even a single locally cooperative unfolding event on the time scale of the experiment (300 s). Under these physiologically relevant conditions, the binding of the cAb-

Table 2: Temperatures of the Transition Midpoint (T_m) Determined by Far-UV CD Measurements in Citrate Buffer (pH 5.5) Containing 3 M Urea

protein	T_m (°C)	protein	T_m (°C)
I56T lysozyme	56 ± 1	cAb-HuL22	49 ± 2
D67H lysozyme	56 ± 1	cAb-HuL2-S54C/I78C	66 ± 1

HuL22 fragment, therefore, inhibits dramatically the locally cooperative unfolding event of both the I56T and D67H variants and hence restores their global cooperativity to that characteristic of the wild-type lysozyme.

cAb-HuL22 Is Not Stable Enough To Inhibit Lysozyme Amyloid Fibril Formation. Given that the reduced cooperativity of the amyloidogenic variants is likely to be a primary factor in their ability to aggregate readily into amyloid fibrils (*10, 12, 13*), binding of the cAb-HuL22 fragment should in principle inhibit the formation of fibrils by restoring the global cooperativity of the lysozyme variants, in a manner similar with that observed with binding of cAb-HuL6 (*10, 13*). Thermal denaturation of cAb-HuL22 followed by far-UV CD under the experimental conditions used to study fibril formation by the variants of lysozyme in vitro [0.1 M citrate buffer (pH 5.5) containing 3 M urea] indicates, however, that the temperature of the midtransition (T_m) of cAb-HuL22 (49 ± 2 °C) is lower than that of the I56T and D67H variants themselves (T_m = 56 ± 1 °C) (Table 2). This result suggests that cAb-HuL22 may not be stable enough to allow the effects of its binding on the aggregation behavior of the lysozyme variants to be monitored reliably. The kinetics of aggregation monitored by the absorbance at 600 nm indicate that the solution containing the D67H protein and cAb-HuL22 (in a 10% molar excess) shows even faster aggregation than that containing only the lysozyme variant (Figure 7A). Furthermore, the final absorbance value at 600 nm of this solution is much higher than that observed in the absence of cAb-HuL22, suggesting that both the nanobody and the lysozyme variant aggregate during this experiment. After incubation for 525 min, aliquots of the solution containing only the D67H variant and that containing both the D67H lysozyme and the nanobody were analyzed by SDS−PAGE, to determine the quantity of soluble protein present (Figure 7B). The results clearly show that both the lysozyme variant and the antibody fragment have aggregated almost completely.

Generation of a More Stable Version of the Antibody Fragment. The single-domain nature of nanobodies makes subsequent molecular manipulations to modify their affinity (*32*), their specificity (*33*) or their conformational stability (*18, 33, 34*) much easier than those of conventional antibody fragments. In particular, it has been shown that the insertion of a disulfide bond at positions 54 and 78 (IMGT numbering) between the two β-sheets that form the core of the protein generally increases the stability of V_HHs without drastically impairing their binding affinity (*18, 34*). Cysteine residues were therefore introduced at positions 54 and 78 in cAb-HuL22, leading to a variant (termed cAb-HuL22-S54C/I78C) with no significant reduction in affinity for the wild-type, I56T, and D67H lysozymes (Table 1).

Thermal denaturation experiments followed by far-UV CD experiments under buffer conditions in which the uncomplexed D67H forms amyloid fibrils [0.1 M citrate buffer (pH 5.5) containing 3 M urea] indicate that the T_m of cAb-HuL22-S54C/I78C is 66 ± 1 °C, a value ~17 °C higher than that

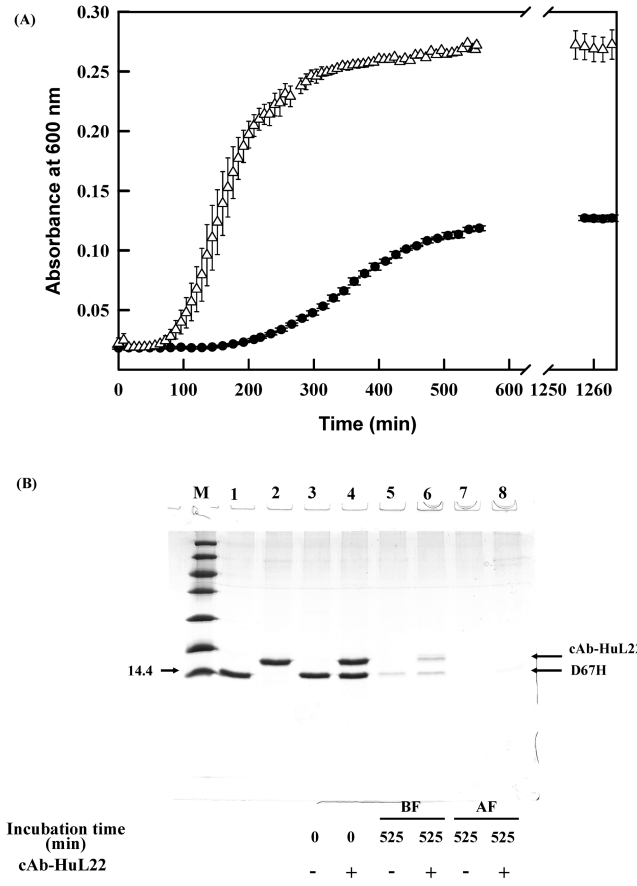

FIGURE 7: Kinetics of aggregation of solutions containing the D67H lysozyme alone and the D67H lysozyme with cAb-HuL22. (A) Time course of the aggregation of a sample containing 6.8 μM D67H (●) and a sample containing 6.8 μM D67H lysozyme and 7.5 μM cAb-HuL22 antibody fragment (△) as monitored by the absorbance at 600 nm. Each kinetic trace is the average of two experiments conducted in duplicate; the error bars indicate the standard error. The data were recorded at 48 °C while the solution was stirred. (B) SDS−PAGE analysis of samples before and after incubation for 525 min (lanes 3−8). BF and AF stand for "before filtration" and "after filtration" through 0.22 mm pore size filters, respectively. After incubation for 525 min, virtually no D67H lysozyme remained in the soluble form both in the absence (lane 7) and in the presence of cAb-HuL22 (lane 8); the cAb-HuL22 had also completely aggregated (lane 8). Comparison of lanes 5 and 7 and lanes 6 and 8 indicates that most of the aggregates formed are SDS-resistant. Equal volumes of D67H (6.8 μM) and cAb-HuL22 (7.5 μM) solutions are shown in lane 1 and 2, respectively; molecular mass markers are shown in lane M.

of its wild-type counterpart [T_m = 49 ± 2 °C (Table 2)]. Most interestingly, it was found that the engineered version of cAb-HuL22 does not aggregate following prolonged incubation under conditions used to form amyloid fibrils with the uncomplexed D67H lysozyme, even at high concentrations (data not shown), making it ideal for investigating the effect of its binding on the aggregation properties of the lysozyme variants.

Engineered cAb-HuL22 Inhibits Human Lysozyme Amyloid Fibril Formation. Using absorbance measurements at 600 nm, we initially monitored the kinetics of aggregation of the D67H protein in the absence and presence of a cAb-HuL22-S54C/I78C:D67H ratio of 3:2 (Figure 8A). In the absence of the antibody fragment, the D67H lysozyme readily aggregates, following a sigmoidal curve characterized by a lag phase of 150 ± 15 min and a half-time of aggregation

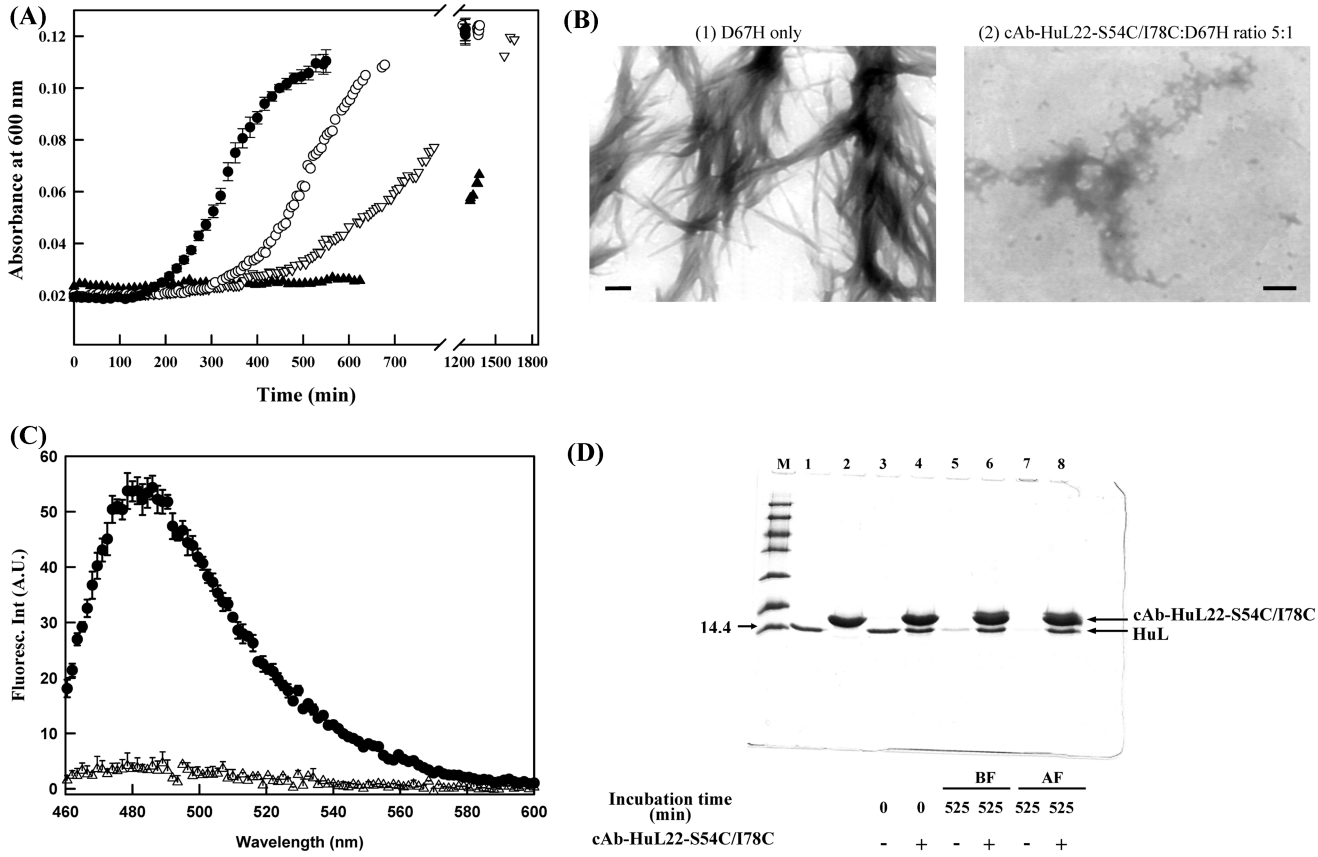

FIGURE 8: Inhibition of lysozyme fibril formation by cAb-HuL22-S54C/I78C. (A) Time course of aggregation of the D67H lysozyme variant in the presence of various ratios of cAb-HuL22-S54C/I78C, monitored by absorbance measurements at 600 nm. In each experiment, the lysozyme concentration was 6.8 μM and the antibody concentration was 0 (●), 10.2 (○), 20.4 (▽), and 34 μM (▲). The data were recorded at 48 °C while the solution was stirred. (B−D) Comparisons of the properties of the sample containing only the D67H lysozyme (6.8 μM) and that containing the D67H lysozyme (6.8 μM) and cAb-HuL22-S54C/I78C (34 μM) after incubation for 525 min. (B) TEM analysis of the samples. The bar represents 200 nm. (C) Thioflavin T fluorescence for D67H lysozyme alone (●) and D67H lysozyme in the presence cAb-HuL22-S54C/I78C (△). (D) SDS−PAGE analysis of samples before and after incubation for 525 min (lanes 3−8). BF and AF stand for before filtration and after filtration through 0.22 mm pore size filters, respectively. Virtually no D67H lysozyme remained in the soluble form in the absence of cAb-HuL22-S54C/I78C (lane 7); in contrast, the majority of lysozyme remained in the soluble form in the sample containing cAb-HuL22-S54C/I78C (lane 8). Again, comparison of lanes 5 and 7 indicates that most of the aggregates formed by the D67H lysozyme are SDS-resistant. Equal volumes of D67H (6.8 μM) and cAb-HuL22-S54C/I78C (34 μM) solutions are shown in lanes 1 and 2, respectively; molecular mass markers are shown in lane M.

of 350 ± 10 min. In the presence of a cAb-HuL22-S54C/I78C:D67H molar ratio of 3:2, the kinetics of aggregation were significantly slowed, the lag phase and the half-aggregation time being 300 ± 15 and 530 ± 15 min, respectively. Contrary to the situation observed in the presence of wild-type cAb-HuL22 (Figure 7A), at the end of the experiment a similar absorbance value was obtained for the samples containing only the lysozyme variant and that containing both the lysozyme variant and cAb-HuL22-S54C/I78C. This result suggests that essentially all the lysozyme molecules eventually aggregate, whereas cAb-HuL22-S54C/I78C remains in solution; this was indeed confirmed by SDS−PAGE analysis (data not shown). The efficiency of the inhibition of aggregation further increases in the presence of higher nanobody:lysozyme molar ratios (Figure 8A). In the presence of a 5-fold molar excess of cAb-HuL22-S54C/I78C, no increase in absorbance was observed after incubation for 600 min; slow aggregation, however, occurs over longer incubation times. The fact that the efficiency of the inhibition increases with the amount of antibody fragment suggests that under fibril forming conditions, the affinity of cAb-HuL22-S54C/I78C is significantly lowered so that a large excess of antibody fragment is necessary to ensure that most of the lysozyme molecules are bound. It is, however, not easy to measure the affinity of cAb-HuL22-S54C/I78C for the D67H lysozyme variant under these conditions (i.e., 3 M urea and 48 °C). The affinity of cAb-HuL22-S54C/I78C for WT-HuL could be measured by ITC (Figure 9A) and was found to be ~20 times lower than that measured at 50 °C in the absence of urea (i.e., 0.94 ± 0.12 μM vs 34 nM). A similar ITC measurement could not be performed under fibril forming conditions for the D67H lysozyme due to the fact that this protein aggregates during the time frame of the experiment. Interestingly, the IC_{50} values measured at 25 °C for both the WT and D67H lysozymes and at 45 °C for WT-HuL are ~3−5 times greater than the K_D values determined by Biacore or ITC measurements (Figure 9B and Table 1). This observation indicates that the affinity of cAb-HuL22-S54C/I78C for D67H lysozyme under conditions near those for forming fibrils could be estimated from the IC_{50} value measured at 45 °C in 0.1 M citrate buffer (pH 5.5) and 3 M urea. The IC_{50} measured was 21 μM (Figure 9B inset), and therefore, the K_D value estimated from it is on the order of 4.5−7 μM, which is good agreement with the results obtained for the inhibition of fibril formation (Figure 8A).

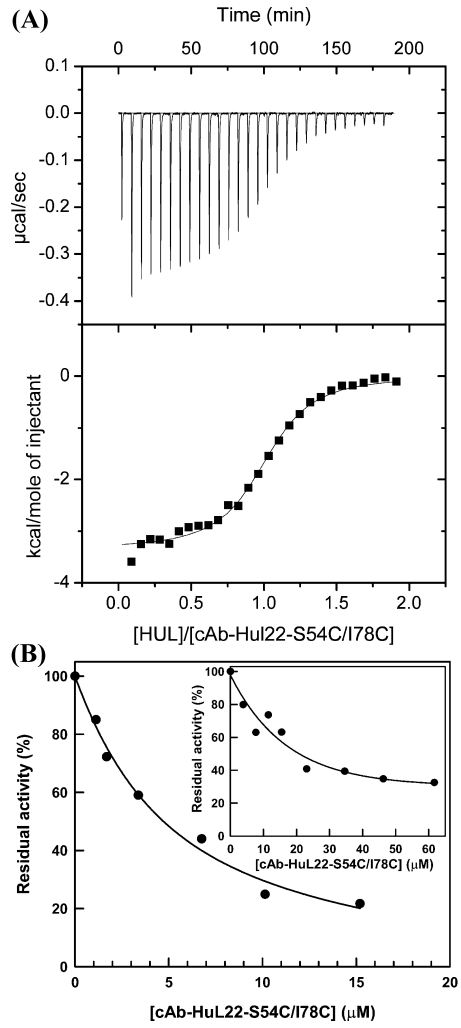

FIGURE 9: Determination of the affinity of cAb-HuL22-S54C/I78C for lysozyme under fibril forming conditions. (A) ITC profile for cAb-HuL22-S54C/I78C−WT-HuL interaction: (top) baseline-corrected instrument response upon titration of 308 μM WT-HuL into 34 μM cAb-HuL22-S54C/I78C and (bottom) normalized integrated data (■) and the best fit of the binding parameters (—). (B) Inhibition of WT-HuL and D67H lysozyme (inset) activity by cAb-HuL22-S54C/I78C at 45 °C in 0.1 M citrate buffer (pH 5.5) containing 3 M urea. The residual activity in the presence of various concentrations of cAb-HuL22-S54C/I78C is plotted relative to that measured in its absence.

The process of aggregation in the presence of a 5:1 nanobody:lysozyme ratio was explored in more detail and compared to that carried out with the D67H lysozyme alone. After incubation for 525 min, both samples were analyzed by transmission electron microscopy (EM) (Figure 8B), and the fluorescence of thioflavin T (Thio-T), an amyloid binding dye, was measured (Figure 8C). Moreover, samples before and after filtration through a 0.22 μm pore size filters were analyzed by SDS−PAGE (Figure 8D). Finally, the amounts of protein remaining in the filtrate were determined by measurement of the absorbance at 280 nm. The results clearly show that, in the absence of the antibody fragment, the D67H lysozyme had almost completely aggregated into amyloid fibrils over this incubation time. However, in the presence of a 5-fold molar excess of cAb-HuL22-S54C/I78C, no such aggregates were observed and a large proportion of the lysozyme and cAb-HuL22-S54C/I78C molecules (>90%) were still present in the solution. Some nonfibrillar aggregates that do not bind Thio-T were observed in the sample in the presence of the nanobody. These species may result from the slow aggregation of the lysozyme variant that became evident at longer incubation times (Figure 8A).

DISCUSSION

In this study, we have selected a nanobody that binds in the active site of human lysozyme via its long CDR3 loop (29 residues) with a high affinity (i.e., $K_D = 34-35$ nM for the WT and I56T lysozymes, and $K_D = 150$ nM for the D67H variant). Moreover, this antibody fragment is a very good lysozyme inhibitor with an IC_{50} value in the nanomolar range.

In the presence of the nanobody, the locally cooperative, albeit transient, unfolding event observed under physiologically relevant conditions, which is characteristic of both amyloidogenic variants of lysozyme (*10, 12*), is strongly inhibited. The result of this binding is a significant inhibition of the lysozyme variants' aggregation. This inhibitory effect is fully consistent with our model (*7*) for formation of fibrils by human lysozyme, in which the formation of the amyloid fibrils is thought to proceed through the partial unfolding of the amylotope (here the region of the structure that encompasses the β-domain and the adjacent C-helix); this process enables self-association to occur by contact with another partially unfolded lysozyme molecule, through the mutually unfolded regions of the polypeptide chain (*7*). Remarkably, the mechanism by which the cAb-HuL22 antibody fragment inhibits the formation of amyloid fibrils is very similar to that observed for cAb-HuL6, the first anti-human lysozyme nanobody characterized (*10, 13*), despite the fact that these two nanobodies recognize different regions of the lysozyme structure (Figure 4B). Previous results suggested that the weakening of the interface region between the α- and β-domains is a critical factor in reducing the global cooperativity of the amyloidogenic lysozyme variants (*9*). This work and previous studies suggest that both cAb-HuL6 and cAb-HuL22 inhibit the locally cooperative unfolding event of the amyloidogenic lysozyme variants by restoring the constraints at the interface between the two domains, and hence by generating a higher degree of interdomain stability. Although no X-ray crystallographic data for the complex between cAb-HuL22 and lysozyme are available, data obtained in this work by NMR and SPR measurements suggest that the epitope of cAb-HuL22 is likely to encompass residues located at the interface between the α- and β-domains. On the other hand, the epitope of cAb-HuL6 is remote from the interface region, and therefore, the stabilization of the interface region by cAb-HuL6 occurs at least in part through the propagation of long-range conformational effects (*13*). Very interestingly, preliminary experiments have shown that the binding of a third nanobody specific for human lysozyme, cAb-HuL5, to the amyloidogenic lysozyme variants does not inhibit the cooperative unfolding of the amylotope. Altogether, these observations suggest that detailed study of the effects of a series of nanobodies directed against different epitopes of lysozyme on the stability and global cooperativity of the lysozyme variants will allow a better understanding of how binding effects propagate to distal regions from the binding site.

Protein misfolding and aggregation are prominent features of many diseases, including systemic amyloidoses

and neurodegenerative disorders, such as Alzheimer's and Parkinson's diseases, type II diabetes, and spongiform encephalopathies (*35*). As a result of the increasingly serious impact of such diseases, especially on the aging population of the developed world, a wide range of strategies is being actively explored for their prevention or treatment (*36*). There is a growing body of evidence which shows that the aggregation process leading to the formation of amyloid fibrils is complex and involves a variety of conformational rearrangements and multiple steps of assemblies (*35*). Many recent results indicate that the fibrils may not be the most toxic species; instead, the latter appear to be relatively small oligomers with high surface-to-volume ratios, which are formed at early stages on the aggregation pathway (*37*). One of the most attractive therapeutic options is, therefore, to prevent the accumulation of aggregation-prone species by inhibiting the process that leads to their formation. Inhibition of amyloid fibril formation via the stabilization of the native state upon binding small molecules or proteins has indeed been demonstrated for several proteins (*10, 13, 38*−*41*). These compounds have been found to function by reducing the level of partially unfolded proteins that are vulnerable to aggregation. Studies of transthyretin, for example, have shown that small molecules mimicking the binding of natural ligands at the interface between subunits are highly promising therapeutic agents [some are in clinical trials (*42*)], because they dramatically slow the initial misfolding event (tetramer dissociation) that is required for partial monomer denaturation and misassembly into amyloid fibrils (*39, 43, 44*). The results presented here constitute another example showing the inhibition of amyloid fibril formation as the result of the stabilization of the native state of an amyloidogenic protein by binding molecules targeted to the binding sites of its natural ligands. A number of misfolding diseases, including amyloidosis, are associated with proteins that carry an enzymatic or transport function (*37*), and therefore, the design of drugs that bind to the regions of these proteins that accommodate their natural ligands can represent a general strategy of therapeutic interest for preventing these diseases in vivo. As shown in this study, a significant reduction in the rate of amyloid fibril formation can be obtained at subsaturation ratios of antibody fragments. For proteins having an essential function, it should therefore be possible to delay significantly the disease, while retaining significant protein activity.

The generation and use of camelid heavy-chain antibody fragments discussed in this work are of particular interest in generating binders that specifically recognize protein binding sites with a high affinity (i.e., in the nanomolar range). It has been shown in a range of studies that a significant fraction of heavy-chain antibodies raised against enzymes interact directly with their active site, indicating that the latter are immunodominant for this class of immunoglobulins (*31, 45, 46*). Moreover, because they are devoid of light chains, the paratope of the heavy-chain antibodies is restricted to three CDRs (instead of six for conventional antibody fragments), of which the CDR3 loop often provides the vast majority (>70%) of the binding surface with the antigen (*14, 46*). This loop, therefore, constitutes a rather simple molecular scaffold for the design of small molecules capable of binding the antigen in a manner analogous to that of the parent antibody. For example, a 26-amino acid residue peptide has been designed from the CDR3 loop of cAb-Lys3 that binds in the active site of hen lysozyme (Figure 4E) (*47*). This peptide was shown to act as a potential enzyme inhibitor by mimicking an oligosaccharide substrate (*47*).

Two recent studies have shown that the introduction of a disulfide bridge into the framework at positions 54 and 78 (IMGT numbering) linking β-strands C′ and D (Figure 4E) impairs neither the expression yield nor the affinity of the V_HHs; however, it significantly increases their conformational stability ($\Delta\Delta G^\circ = 10$ kJ/mol) and their thermostability ($\Delta T_m \sim 10$ °C) (*18, 34*). In this work, we have shown that the variant of cAb-HuL22 containing an additional disulfide bound at positions 58 and 74, denoted cAb-HuL22-S54C/I78C, is also significantly more thermostable than its parental counterpart; its T_m in 0.1 M citrate buffer (pH 5.5) in the presence of 3 M urea is 17 °C higher than that of wild-type cAb-HuL22 (Table 2). Moreover, we have shown that the propensity of cAb-HuL22-S54C/I78C to aggregate is significantly reduced and its functionality maintained when incubated under even very harsh conditions (i.e., in the presence of 3 M urea at 48 °C). These results support the idea that the introduction of an additional disulfide bond between the two β-sheets forming the hydrophobic core of V_HHs can be used as a general strategy to stabilize them and thus generate functionality over a very wide range of stringent conditions. For many proteins, it is necessary to use conditions such as low pH, high temperature, or moderate concentrations of chemical denaturants to increase considerably the rates at which they aggregate in vitro. Given their unique properties, including their small size (115−140 amino acids), high specificity, solubility, and stability, and the ease by which they can be generated and genetically modified to improve their properties, camelid antibody fragments are, therefore, of special interest as structural probes for investigating the mechanism of aggregation and as potential inhibitors of fibril formation.

ACKNOWLEDGMENT

We thank Andrew Spencer, Marcos Alcocer, and Fredrick Holmqvist for assistance in expression and purification of human lysozymes. We thank J.-M. Frère for many helpful discussions and critical reading of the manuscript.

REFERENCES

1. Pepys, M. B., Hawkins, P. N., Booth, D. R., Vigushin, D. M., Tennent, G. A., Soutar, A. K., Totty, N., Nguyen, O., Blake, C. C., Terry, C. J., Feest, T. G., Zalin, A. M., and Hsuan, J. J. (1993) Human lysozyme gene mutations cause hereditary systemic amyloidosis. *Nature 362*, 553–557.
2. Rocken, C., Becker, K., Fandrich, M., Schroeckh, V., Stix, B., Rath, T., Kahne, T., Dierkes, J., Roessner, A., and Albert, F. W. (2006) ALys amyloidosis caused by compound heterozygosity in exon 2 (Thr70Asn) and exon 4 (Trp112Arg) of the lysozyme gene. *Hum. Mutat. 27*, 119–120.
3. Valleix, S., Drunat, S., Philit, J. B., Adoue, D., Piette, J. C., Droz, D., MacGregor, B., Canet, D., Delpech, M., and Grateau, G. (2002) Hereditary renal amyloidosis caused by a new variant lysozyme W64R in a French family. *Kidney Int. 61*, 907–912.
4. Yazaki, M., Farrell, S. A., and Benson, M. D. (2003) A novel lysozyme mutation Phe57Ile associated with hereditary renal amyloidosis. *Kidney Int. 63*, 1652–1657.

5. Dumoulin, M., Bellotti, V., and Dobson, C. M. (2005) Hereditary systemic amyloidosis associated with mutational variants of human lysozyme. In *The beta pleated sheet conformation and diseases* (Sipe, J. D., Ed.) pp 635−656, VCH Verlag GmbH & KgaA, Weinheim, Germany.
6. Dumoulin, M., Johnson, J. R. K., Bellotti, V., and Dobson, C. M. (2007) Human lysozyme. In *Protein Misfolding, Aggregation, and Conformational Diseases* (Uversky, V. N., and Fink, A., Eds.) pp 285−308, Springer, New York.
7. Dumoulin, M., Kumita, J. R., and Dobson, C. M. (2006) Normal and aberrant biological self-assembly: Insights from studies of human lysozyme and its amyloidogenic variants. *Acc. Chem. Res. 39*, 603–610.
8. Blake, C. C., and Swan, I. D. (1971) X-ray analysis of structure of human lysozyme at 6 Å resolution. *Nat. New Biol. 232*, 12–15.
9. Booth, D. R., Sunde, M., Bellotti, V., Robinson, C. V., Hutchinson, W. L., Fraser, P. E., Hawkins, P. N., Dobson, C. M., Radford, S. E., Blake, C. C., and Pepys, M. B. (1997) Instability, unfolding and aggregation of human lysozyme variants underlying amyloid fibrillogenesis. *Nature 385*, 787–793.
10. Dumoulin, M., Canet, D., Last, A. M., Pardon, E., Archer, D. B., Muyldermans, S., Wyns, L., Matagne, A., Robinson, C. V., Redfield, C., and Dobson, C. M. (2005) Reduced global cooperativity is a common feature underlying the amyloidogenicity of pathogenic lysozyme mutations. *J. Mol. Biol. 346*, 773–788.
11. Funahashi, J., Takano, K., Ogasahara, K., Yamagata, Y., and Yutani, K. (1996) The structure, stability, and folding process of amyloidogenic mutant human lysozyme. *J. Biochem. (Tokyo, Jpn.) 120*, 1216–1223.
12. Canet, D., Last, A. M., Tito, P., Sunde, M., Spencer, A., Archer, D. B., Redfield, C., Robinson, C. V., and Dobson, C. M. (2002) Local cooperativity in the unfolding of an amyloidogenic variant of human lysozyme. *Nat. Struct. Biol. 9*, 308–315.
13. Dumoulin, M., Last, A. M., Desmyter, A., Decanniere, K., Canet, D., Larsson, G., Spencer, A., Archer, D. B., Sasse, J., Muyldermans, S., Wyns, L., Redfield, C., Matagne, A., Robinson, C. V., and Dobson, C. M. (2003) A camelid antibody fragment inhibits the formation of amyloid fibrils by human lysozyme. *Nature 424*, 783–788.
14. Muyldermans, S. (2001) Single domain camel antibodies: Current status. *J. Biotechnol. 74*, 277–302.
15. Cortez-Retamozo, V., Backmann, N., Senter, P. D., Wernery, U., De Baetselier, P., Muyldermans, S., and Revets, H. (2004) Efficient cancer therapy with a nanobody-based conjugate. *Cancer Res. 64*, 2853–2857.
16. Conrath, K. E., Lauwereys, M., Galleni, M., Matagne, A., Frere, J. M., Kinne, J., Wyns, L., and Muyldermans, S. (2001) β-Lactamase inhibitors derived from single-domain antibody fragments elicited in the camelidae. *Antimicrob. Agents Chemother. 45*, 2807–2812.
17. Arbabi Ghahroudi, M., Desmyter, A., Wyns, L., Hamers, R., and Muyldermans, S. (1997) Selection and identification of single domain antibody fragments from camel heavy-chain antibodies. *FEBS Lett. 414*, 521–526.
18. Saerens, D., Conrath, K., Govaert, J., and Muyldermans, S. (2008) Disulfide bond introduction for general stabilization of immunoglobulin heavy-chain variable domains. *J. Mol. Biol. 377*, 478–488.
19. Johnson, R. J., Christodoulou, J., Dumoulin, M., Caddy, G. L., Alcocer, M. J., Murtagh, G. J., Kumita, J. R., Larsson, G., Robinson, C. V., Archer, D. B., Luisi, B., and Dobson, C. M. (2005) Rationalising lysozyme amyloidosis: Insights from the structure and solution dynamics of T70N lysozyme. *J. Mol. Biol. 352*, 823–836.
20. Spencer, A., Morozova-Roche, L. A., Noppe, W., MacKenzie, D. A., Jeenes, D. J., Joniau, M., Dobson, C. M., and Archer, D. B. (1999) Expression, purification, and characterization of the recombinant calcium-binding equine lysozyme secreted by the filamentous fungus *Aspergillus niger*: Comparisons with the production of hen and human lysozymes. *Protein Expression Purif. 16*, 171–180.
21. Dumoulin, M., Conrath, K., Van Meirhaeghe, A., Meersman, F., Heremans, K., Frenken, L. G., Muyldermans, S., Wyns, L., and Matagne, A. (2002) Single-domain antibody fragments with high conformational stability. *Protein Sci. 11*, 500–515.
22. Pace, C. N., and Scholtz, M. (1997) Measuring the conformational stability of a protein. In *Protein structure: A practical approach* (Creighton, T. E., Ed.) pp 299−321, IRL Press, Oxford, U.K.
23. Ohkubo, T., Taniyama, Y., and Kikuchi, M. (1991) ^{1}H and ^{15}N NMR study of human lysozyme. *J. Biochem. (Tokyo, Jpn.) 110*, 1022–1029.
24. Buck, M., Schwalbe, H., and Dobson, C. M. (1995) Characterization of conformational preferences in a partly folded protein by heteronuclear NMR spectroscopy: Assignment and secondary structure analysis of hen egg-white lysozyme in trifluoroethanol. *Biochemistry 34*, 13219–13232.
25. Redfield, C., and Dobson, C. M. (1988) Sequential ^{1}H NMR assignments and secondary structure of hen egg white lysozyme in solution. *Biochemistry 27*, 122–136.
26. Kumagai, I., Sunada, F., Takeda, S., and Miura, K. (1992) Redesign of the substrate-binding site of hen egg white lysozyme based on the molecular evolution of C-type lysozymes. *J. Biol. Chem. 267*, 4608–4612.
27. Kumeta, H., Miura, A., Kobashigawa, Y., Miura, K., Oka, C., Nemoto, N., Nitta, K., and Tsuda, S. (2003) Low-temperature-induced structural changes in human lysozyme elucidated by three-dimensional NMR spectroscopy. *Biochemistry 42*, 1209–1216.
28. Harata, K. (1994) X-ray structure of a monocyclic form of hen egg-white lysozyme crystallized at 313 K. Comparison of two independent molecules. *Acta Crystallogr. D50*, 250–257.
29. Desmyter, A., Transue, T. R., Ghahroudi, M. A., Thi, M. H., Poortmans, F., Hamers, R., Muyldermans, S., and Wyns, L. (1996) Crystal structure of a camel single-domain VH antibody fragment in complex with lysozyme. *Nat. Struct. Biol. 3*, 803–811.
30. Desmyter, A., Spinelli, S., Payan, F., Lauwereys, M., Wyns, L., Muyldermans, S., and Cambillau, C. (2002) Three camelid VHH domains in complex with porcine pancreatic α-amylase. Inhibition and versatility of binding topology. *J. Biol. Chem. 277*, 23645–23650.
31. Muyldermans, S., and Lauwereys, M. (1999) Unique single-domain antigen binding fragments derived from naturally occurring camel heavy-chain antibodies. *J. Mol. Recognit. 12*, 131–140.
32. De Genst, E., Handelberg, F., Van Meirhaeghe, A., Vynck, S., Loris, R., Wyns, L., and Muyldermans, S. (2004) Chemical basis for the affinity maturation of a camel single domain antibody. *J. Biol. Chem. 279*, 53593–53601.
33. Saerens, D., Pellis, M., Loris, R., Pardon, E., Dumoulin, M., Matagne, A., Wyns, L., Muyldermans, S., and Conrath, K. (2005) Identification of a universal VHH framework to graft non-canonical antigen-binding loops of camel single-domain antibodies. *J. Mol. Biol. 352*, 597–607.
34. Hagihara, Y., Mine, S., and Uegaki, K. (2007) Stabilization of an immunoglobulin fold domain by an engineered disulfide bond at the buried hydrophobic region. *J. Biol. Chem. 282*, 36489–36495.
35. Stefani, M., and Dobson, C. M. (2003) Protein aggregation and aggregate toxicity: New insights into protein folding, misfolding diseases and biological evolution. *J. Mol. Med. 81*, 678–699.
36. Rochet, J. C. (2007) Novel therapeutic strategies for the treatment of protein-misfolding diseases. *Expert Rev. Mol. Med. 9*, 1–34.
37. Chiti, F., and Dobson, C. M. (2006) Protein misfolding, functional amyloid and human disease. *Annu. Rev. Biochem. 75*, 333–366.
38. Chiti, F., Taddei, N., Stefani, M., Dobson, C. M., and Ramponi, G. (2001) Reduction of the amyloidogenicity of a protein by specific binding of ligands to the native conformation. *Protein Sci. 10*, 879–886.
39. Hammarstrom, P., Wiseman, R. L., Powers, E. T., and Kelly, J. W. (2003) Prevention of transthyretin amyloid disease by changing protein misfolding energetics. *Science 299*, 713–716.
40. Johnson, S. M., Wiseman, R. L., Sekijima, Y., Green, N. S., Adamski-Werner, S. L., and Kelly, J. W. (2005) Native state kinetic stabilization as a strategy to ameliorate protein misfolding diseases: A focus on the transthyretin amyloidoses. *Acc. Chem. Res. 38*, 911–921.
41. Ray, S. S., Nowak, R. J., Brown, R. H., Jr., and Lansbury, P. T., Jr. (2005) Small-molecule mediated stabilization of familial amyo-

trophic lateral sclerosis linked superoxide dismutase mutants against unfolding and aggregation. *Proc. Natl. Acad. Sci. U.S.A. 102*, 3639–3644.
42. Merlini, G., and Bellotti, V. (2005) Lysozyme: A paradigmatic molecule for the investigation of protein structure, function and misfolding. *Clin. Chim. Acta 357*, 168–172.
43. Foss, T. R., Wiseman, R. L., and Kelly, J. W. (2005) The pathway by which the tetrameric protein transthyretin dissociates. *Biochemistry 44*, 15525–15533.
44. Foss, T. R., Kelker, M. S., Wiseman, R. L., Wilson, I. A., and Kelly, J. W. (2005) Kinetic stabilization of the native state by protein engineering: Implications for inhibition of transthyretin amyloidogenesis. *J. Mol. Biol. 347*, 841–854.
45. Transue, T. R., De Genst, E., Ghahroudi, M. A., Wyns, L., and Muyldermans, S. (1998) Camel single-domain antibody inhibits enzyme by mimicking carbohydrate substrate. *Proteins 32*, 515–522.
46. De Genst, E., Silence, K., Decanniere, K., Conrath, K., Loris, R., Kinne, J., Muyldermans, S., and Wyns, L. (2006) Molecular basis for the preferential cleft recognition by dromedary heavy-chain antibodies. *Proc. Natl. Acad. Sci. U.S.A. 103*, 4586–4591.
47. Marquardt, A., Muyldermans, S., and Przybylski, M. (2006) A Synthetic Camel Anti-Lysozyme Peptide Antibody (Peptibody) with Flexible Loop Structure Identified by High-Resolution Affinity Mass Spectrometry. *Chemistry 12*, 1915–1923.
48. Koradi, R., Billeter, M., and Wuthrich, K. (1996) MOLMOL: A program for display and analysis of macromolecular structures. *J. Mol. Graphics 14*, 51–55, 29−32.

BI8005797